Experimental overview of Ni + Ni collisions at 32 MeV/nucleon : discriminant analysis and duality in the decay modes of a fusion-like system.

P. Lautesse,[1] A.M. Maskay,[1] E. Gerlic,[1] P. Désesquelles,[2] J.L. Laville,[3] O. Lopez,[3]
G. Auger,[4] B. Borderie,[2] R. Bougault,[3] B. Bouriquet,[4] J.L. Charvet,[5] A.
Chbihi,[4] J. Colin,[3] D. Cussol,[3] R. Dayras,[5] N. de Cesare,[6] A. Demeyer,[1]
D. Durand,[3] J.D. Frankland,[4] E. Galichet,[2, 7] D. Guinet,[1] B. Guiot,[4] S. Hudan,[4]
F. Lavaud,[2] J.F. Lecolley,[3] N. Le Neindre,[4] L. Nalpas,[5] J. Normand,[3] M. Pârlog,[8]
E. Plagnol,[2] M. F. Rivet,[2] E. Rosato,[6] R. Roy,[9] C. Schmitt,[4, *] J.C. Steckmeyer,[3]
B. Tamain,[3] K. Turzo,[1] E. Vient,[3] M. Vigilante,[6] C. Volant,[5] and J.P. Wieleczko[4]

(INDRA collaboration)

[1] *Institut de Physique Nucléaire, IN2P3-CNRS et Université F-69622 Villeurbanne, France.*
[2] *Institut de Physique Nucléaire, IN2P3-CNRS, F-91406 Orsay Cedex, France.*
[3] *LPC, IN2P3-CNRS, ISMRA et Université, F-14050 Caen Cedex, France.*
[4] *GANIL, CEA et IN2P3-CNRS, B.P. 5027, F-14076 Caen Cedex, France.*
[5] *DAPNIA/SPhN, CEA/Saclay, F-91191 Gif sur Yvette, France.*
[6] *Dip. di Scienze Fisiche e Sez. INFN,*
Univ. di Napoli "Federico II", Napoli, Italy.
[7] *Conservatoire National des Arts et Métiers, F-75141 Paris Cedex 03.*
[8] *Nat. Inst. for Physics and Nuclear Engineering, Bucharest-Măgurele, Romania.*
[9] *Laboratoire de Physique Nucléaire, Université Laval, Québec, Canada.*

^{58}Ni+^{58}Ni collisions at 32 MeV/nucleon have been studied with the 4 π multidetector INDRA. The evolution from binary (dissipative) collisions to a fusion-like process is evidenced with decreasing impact parameter throughout a set of experimental observables within a Discriminant Analysis. Pre-equilibrium effects and characteristics of a single-source emission are discussed. A coexistence (bimodality) between two decay mechanisms is pointed out and examined in the context of a multiple-fragment (particle) emission.

PACS numbers: 25.70.-z, 25.70.Lm, 25.70.Pq

I. INTRODUCTION

Reaction processes implying the formation and the decay of a hot composite nucleus including most of the incident nucleons, constitute a non negligible contribution to the cross-section of central collisions between heavy ions around Fermi energy[1]-[11]. The concerned incident energy range, often referred to as "intermediate energies", runs from above the Coulomb barrier up to about 100 MeV/nucleon, where individual nucleon-nucleon collisions effects overcome mean field effects. In that wide energy domain, a beam energy value of 32 MeV/nucleon - close to the Fermi one - appears to be well suited to produce these intermediate subsystems, since it stands far enough from the Coulomb regime while being not too high for the aforementioned effects to take place. At that energy, it is well known that the complete fusion process - which ends

up in a cold heavy residue storing the whole initial mass but some evaporation particles - has vanished [5, 6] and is replaced by collisions leading to dominant multi-source events. Nevertheless the formation of hot, composite subsystems has been evidenced in various experimental data involving central collisions, mainly in heavy (e.g. Xe+Sn [3]) and very heavy (e.g. Au+Au [10], Gd+U [9]) systems. They appear to be highly excited - typically above 5 MeV/nucleon - and their sizes are close to the total incident mass (projectile+target nuclei) except for the fraction emitted in the pre-equilibrium phase. Above an excitation energy of about 3 - 5 MeV/nucleon, their decay occurs with a relatively abundant production of fragments with charge Z$\geq$3. Moreover these subsystems appear to have reached a high degree of thermalization since many observables seem to be mainly driven by statistical decay. Therefore, it is fundamental to understand the reaction mechanisms which lead to such an extreme situation : how is it possible to create an intermediate subsystem which concentrates almost the whole initial mass and presumably reaches thermal equilibrium in a rather short

*Present address: GSI mbH, D-64291 Darmstadt, Germany.

time ? Do we deal with a more and more unstable incomplete fusion system or with a completely different mechanism?

In order to analyze this hot source, it is necessary to eliminate non equilibrated components which might contaminate the exit channel. Indeed, dynamical models [12] suggest that out-of-equilibrium nucleon emission may occur at various stages of the reaction, as confirmed by experiment [13] ; such processes are often referred to as pre-equilibrium emission [4, 14]. One aspect of pre-equilibrium emission has been recently evidenced as a "spray" [7] which implies forward production of not only light particles but also light fragments. A deeper and more realistic overall insight on these processes requires exclusive experiments performed with a multidetector array and a good discrimination of single-source events. Thus a specific procedure able to isolate the single-source subset from major contributions due to multi-source events is necessary. Such a procedure has been widely discussed in a previous paper [15], where the quality of the resulting sample of single-source events has been shown. We even deduced a reliable "fusion-like" cross-section of 170 ± 20 mb for the ^{58}Ni+^{58}Ni reaction at 32 MeV/nucleon [2, 15].

In the present paper, we report on an investigation of such reaction mechanism(s) including a persistent fusion-like process in these 32 MeV/nucleon ^{58}Ni+^{58}Ni collisions. One of the underlying purposes is to determine to what extent the system has forgotten the entrance channel, i.e. how far this fusion-like source might be considered as a hot composite nucleus.

After a short description of the experimental procedure involving the multidetector INDRA (Sec. II), we shall study in a more refined way the performances of the new discriminant variable, d_{625}, throughout the experimental evolution of various observables, in order to characterize the single-source events selected among dominant poly-source ones (Sec. III). Then, the hypothesis of the fusion-like nucleus at thermal equilibrium will be verified and the pre-equilibrium emission will be characterized (Sec. IV). Finally Sec. V will be devoted to the decay properties of the hot source and followed by conclusions in Sec. VI.

II. EXPERIMENTAL DETAIL

The experiment was performed at GANIL, with the ^{58}Ni^{24+} beam at 32 MeV/nucleon impinging on a 179 μg/cm^2 ^{58}Ni target. Events were recorded by the INDRA charged products multidetector. As INDRA's characteristics are exhaustively described in a technical paper [16], we only recall here its main features. INDRA is an ensemble of 336 detection cells arranged in 17 rings ; the first one (2°-3°) is a phoswich array of plastic scintillators. Rings 2 to 9 (i.e. for polar angles ranging from 3° to 45°) consist in three level telescopes including an ionization chamber(IoCh) followed by a solid state silicon detector(Si) and a caesium iodide scintillator, CsI(Tl). The medium and backward angular range (45° to 176°) is restricted to IoCh/CsI moduli. The multiplicity triggering condition was set to a minimum of four detectors firing per event, ($M \geq 4$), in order to eliminate the most peripheral collisions. The whole INDRA device provides a detection, identification and energy measurement with a 90% of 4π geometrical efficiency.

Figure 1 presents the diagram of the total reconstructed momentum ($P_{tot} = \sum_{j=1}^{Mult} m_j |v_j|$, where j is the fragment (or light particle) number in a given event with multiplicity *Mult*) versus the total charge (Z_{tot}) detected by INDRA. One sees that quite full efficiency is achieved, provided we use a subset of "complete" events as in zone γ, characterized by a performant detection involving $\geq 80\%$ of the initial charge (Z_{ini}) and momentum (P_{ini}). The α and β zones correspond to events when a large part of the charge and/or momentum is missed. The present study is then restricted to that subset γ of complete events, excluding the most peripheral collisions, which represents about 13% of the detected events.

Figure 2 displays a set of charge versus energy maps for each identification level allowed by INDRA : they illustrate the three kinds of ΔE-E telescope contributions. These maps exhibit the charge-energy plots for fragments detected over the whole 4π acceptance. Particle and fragment identification is obtained on the full charge/energy range concerned by these Ni + Ni collisions at 32 MeV/nucleon. The left column, related to IoCh/Si maps, is devoted to slow (mostly heavy) fragments detected at forward angles ($\leq 45^o$). The middle column displays Si/CsI maps, for faster and lighter fragments, also detected at forward angles. Finally, the right column displays
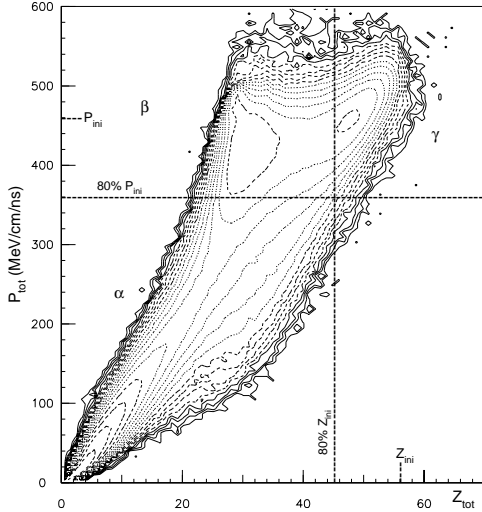
Figure 1: Total charge versus total momentum detected by INDRA for the ^{58}Ni+^{58}Ni system at 32 MeV/nucleon. Z_{ini} and P_{ini} are the initial values of total charge and momentum (axis z with a logarithmic scale). Limits of γ zone are shown to represent the selected set of complete events (see text).

Figure 2: Energy versus Charge ($Z>4$) maps for each Z identification level as described in the text. The three columns stand for the three kinds of ΔE-E telescope arrangements, while the three rows display the three types of events, i.e complete events and complete events with single-source (poly-source) selection, respectively.

IoCh/CsI maps, with fragments detected at larger angles ($\geq 45^o$). The light products, $Z = 1$ to 4 (not shown), are isotopically identified by the Si/CsI telescopes or the CsI alone.

In another way, the top row of Fig. 2 is devoted to "pure single-source events", the middle row to "pure poly-source events" and the bottom one to the whole sample of complete events under study. One can see that all products are very well characterized in charge and energy. The "single-source" and "poly-source" selections are explicited in the next section. We already stress the very different pattern of the charge-energy maps of the top row, (single source events), compared with the two other rows.

III. SINGLE-SOURCE DISCRIMINATION : EXPERIMENTAL OVERVIEW

In this section, we report on a set of observables directly built up from the experimental data, with the aim of establishing the capability of the Discriminant Analysis (D.A.) [17] method to disentangle the various mechanisms involved in a selected sample of events. The uttermost purpose is to study the characteristics of the fusion-like system formed in the reaction.
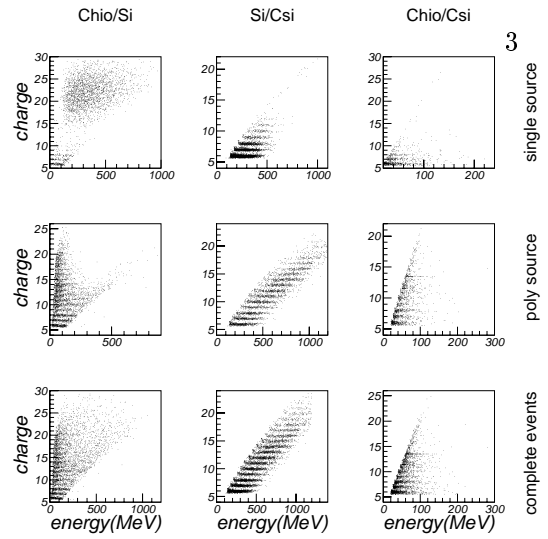
We briefly recall in section A) this D.A. method involving multivariate moments and used to separate the single-source component from the poly-source components. In order to evaluate the discrimination efficiency of the procedure, one needs to go through a stage of simulation for which we have used the event generator Simon [18, 19]. It provides a realistic simulation of heavy-ion collisions at intermediate energies. The Simon code describes the overall reaction process, including the entrance channel dynamics over the full impact parameter range, thus leading to either a binary or a fused system formation within a sharp cut-off description. The decay of the resulting subsystems is described within a sequential emission framework. Outgoing fragments and particles are driven in the final Coulomb field. The code has been shown in [2, 15] to provide a qualitative agreement with the present experimental distributions of static, kinetic and shape observables, therefore constituting a good tool to develop such a discriminant analysis procedure. The generated events are finally filtered according to the multidetector response function. Finally the experimental events are sorted out into four classes according to the resulting discriminant variable, d_{625}. Then static and kinematic experimental observables are analyzed for

those classes in section B).

A. Discriminant Analysis method and resulting d_{625} variable

This original method used to separate a single-source component from other contributions has been recently developped ([2], [15]). It is applied here to the whole set of complete events as defined above and follows a two-step procedure :

i) Firstly, a sub-space describing in an optimum way the experimental information is chosen.
   The basis vectors of this sub-space are the so-called multivariate moments, defined as :

$$M_{jklm} = \sum_{\nu=1}^{Mult} E_A^j(\nu)\ E_x^k(\nu)E_y^l(\nu)E_z^m(\nu),$$

where ν is the fragment (or light particle) number in a given event with multiplicity *Mult*. The mass energy of the νth product is noted E_A and E_x, E_y, E_z are defined by $E_i = E_{kin}\cos\theta_i$, E_{kin} being the kinetic energy in the laboratory frame, θ_i the laboratory angle between the hit detector and axis i with $i \in \{x, y, z\}$, and z the beam axis.

ii) Secondly, the most suitable linear combination of these multivariate moments to provide the best discrimination between single and poly-source events, is searched for using a D.A. technique.

The best deduced linear combination of the 625 first quadrimoments $\{M_{jklm \in \{0,...4\}}\}$, is called the d_{625} variable (with $d_{625} = \sum_{(j,k,l,m)=0}^{4} \alpha_{jklm} M_{jklm}$). Moreover 625 was checked as the number of multivariate moments needed to obtain the amount of information required to significantly describe the whole set of data.
It is worth reminding that the discriminant power and overlap parameters of this d_{625} variable have been proved to be much more efficient compared to the commonly used selection variables such as the isotropy ratio or the flow angle. This is true at least regarding the Ni+Ni system at 32 MeV/nucleon. Furthermore, we emphasize that a larger event sample is obtained in most cases when the event selection is performed with the d_{625} variable instead of the usual global variables.

B. Evolution of some experimental characteristics of the 32 MeV/nucleon Ni+Ni collisions as a function of the d_{625} variable value

In this section, we show that the D.A. procedure is a powerful tool to characterize reaction mechanisms evolving from fusion-like to binary-like collisions. We study this evolution through a set of significant experimental individual and global variables.

We have already shown in [15] that the experimental single source sample belongs to a low impact parameter range (b≤3 fm) compared to the maximum experimental value, 7.5 fm, imposed by the complete event selection, the geometric value being $b_{max} = 9.94$ fm. However, although a separation between the single/poly-source components was clearly observable, the analysis has pointed out that even in the central region of impact parameters (1∼3 fm) where the single-source component is dominant, some contamination with poly-source events was still present.

In the present work, the optimized experimental d_{625} distribution is divided, as shown in Fig. 3 (top row), into four adjacent regions (a, b, c and d) ranging from a pure single-source sample a) to a pure poly-source one d). The bins b) and c) are different mixtures of both contributions. A pure class is defined as a sample being contaminated by less than 3% of events of the other class. The limits of these cuts are deduced, as presented in [15], from a detailed study of the experimental d_{625} two-component distribution, fitted with the sum of two Gaussians. Each of these four slices amounts to ∼50% of the relevant Gaussian.
Figs. 3 and 4 display the evolution of some typical static and kinetic variables gated by these d_{625} cuts.

1. Static variables

Figure 3 is concerned by the evolution of some static variables, charge Z, Z_{max}, Z_{max-1}, and asymmetry distributions, as a function of the d_{625} intervals.
- The *charge distributions f(Z)* show a clear evolution from column a_1) to d_1). The pure
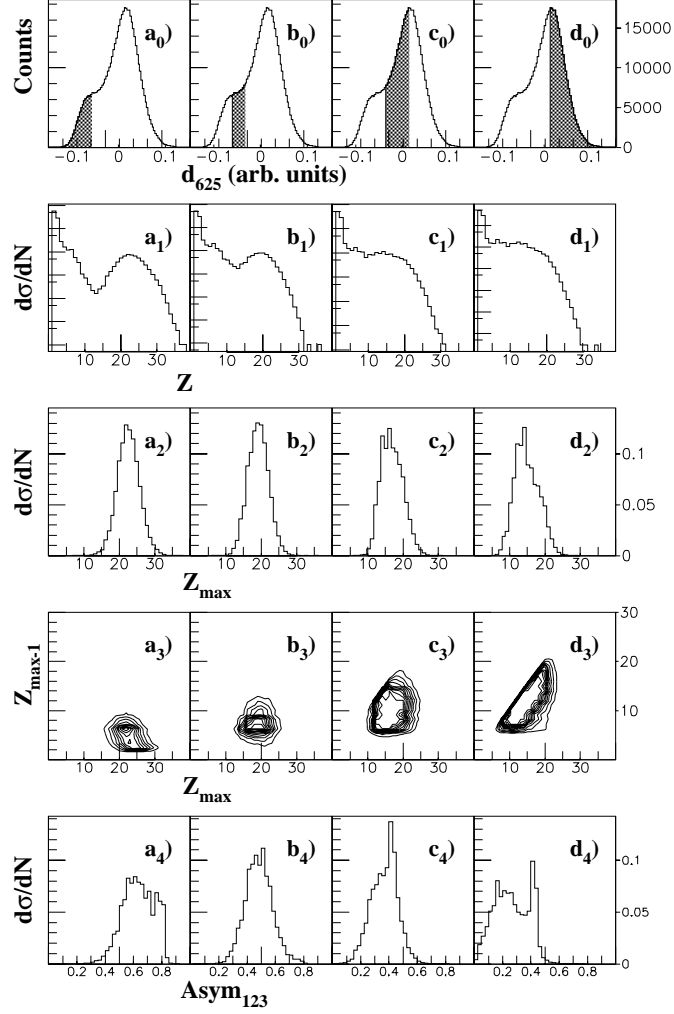
Figure 3: *Static variable* evolution, according to the four (a_0 - d_0) intervals (as shown on top row) forming the whole d_{625} distribution. Corresponding plots are displayed for : Z-charge (a_1 - d_1), Z_{max} charge in the event (a_2 - d_2), correlation of the two heaviest fragments (a_3 - d_3) (axis z with a logarithmic scale), $Asym_{123}$ (a_4 - d_4) (see text).

single-source in a_1) slice, seems to consist essentially in events including on one hand, relatively heavy fragments peaking around $Z \sim 22$ and extending up to $Z \sim 35$ which could be assimilated to incomplete fusion residues and, on the other hand, numerous light products. A pronounced depletion for fragments with $Z \sim 10$ to 15 is clearly observed in a_1), which progressively vanishes from b_1) to d_1) regions. Pure poly-source charge distributions appear to be formed of a plateau between $Z \sim 6$ and $Z \sim 20$, and a tail extending up to $Z \sim 30$.

- The distributions of Z_{max} for each event, a_2) to d_2), reinforce the previous observations :

from the curve a_2), Z_{max} points clearly at ~ 22, the distribution extending from ~ 12 to ~ 32, compared to Z_{tot}=56, suggesting a high energy dissipation. Then for d_2) the Z_{max} mean value decreases down to $\langle Z_{max} \rangle \sim 14$, with a distribution extending from ~ 6 to ~ 25. This latter experimental curve indeed suggests two main Gaussian contributions, i.e. a dominant one with $\langle Z_{max} \rangle \sim 12$ only, and a smaller one with $\langle Z_{max} \rangle \sim 18$, thus reflecting clearly two classes of events in the d_2) cut. Note that the dominant contribution indeed corresponds to more dissipative events than the other one.

- The *charge correlation* between the two

heaviest fragments of the events is displayed from a_3) to d_3). In the d_3) sample, they appear mainly concentrated along the line $Z_{max-1} \sim Z_{max}$, as expected for dominant binary-like collisions of a symmetric system. On the opposite, the single-source sample a_3) presents a bulk which corresponds to expected residues but with most values of Z_{max} running globally from $Z_{max} \sim 20$ up to ~ 27, combined with lighter fragments belonging to 2 islets pointing around $Z \sim 3$ and $Z \sim 6$. Note that the Z_{max-1} value never exceeds ~ 12. These features reflect once more the probable formation of a hot fusion-like nucleus since the Z_{max} residue-like has a relatively small size and is accompanied by numerous light fragments and/or particles. One can note in addition the significant gradual vanishing, from single-source to poly-source samples, of the very light Z_{max-1} products of the first islet ($Z<4$).

- The *charge asymmetry* variable [20] ($Asym_{123}$), which yields a more refined insight into the contents of an event, is defined as :

$$Asym_{123} = \sqrt{\sum_{n=1}^{3}(Z_{max_n} - <Z>)^2/(\sqrt{6}<Z>)},$$

where Z_{max_n} ($Z_{max_1} \geq Z_{max_2} \geq Z_{max_3}$) are the charges of the three heaviest products of an event, and $<Z>$ is their mean value. The variable $Asym_{123}$ reflects the symmetry of the charge partition : values close to 0 stand for nearly equal sizes while values close to 1 imply a heavy fragment plus two light charged products. The medium case ($Asym_{123} \sim 0.5$) then corresponds to the combination of two close size fragments and a light particle. The evolution of the variable $Asym_{123}$ is shown in the bottom part of Fig. 3 from a_4) to d_4). In the poly-source case, d_4), the $Asym_{123}$ extends up to ~ 0.5 and the strong narrow peak pointing at ~ 0.45 corresponds to a binary-like dominant character of the reaction. That feature comes from the less dissipative collisions involving the $Z_{max} \sim Z_{max-1} \sim 17$ component dicussed above. On the other hand the broad bump around the low value of $Asym_{123} \sim 0.2$ reflects products emitted from a more dissipative mid-peripheral process as just proposed above for the numerous events pointing at around $Z_{max-1} \sim Z_{max} \sim 12$ (Figs. d_2), d_3)). The distribution extends down to $Asym_{123} \sim 0$ thus towards some few events with lighter and lighter fragments approaching the same size. Hence they appear as issued from strongly excited poly-sources, or from a very elongated excited single source. At reverse, the single-source plot, a_4), behaves in a very different way since it exhibits a quite broad distribution extending from $Asym_{123} \sim 0.3$ to about 0.85. The main structure is peaking around 0.6, while a weaker structure appears at the highest experimental $Asym_{123}$ values (~ 0.8), typical of an evaporative process.

It can be summarized that the strong variations, from a) to d), of the Z and Z_{max} distributions, together with the charge correlation between the two heaviest fragments in each event and the evolution of the asymmetry variable ($Asym_{123}$), are strongly suggesting a change in the collision process.
These trends are also corroborated by *the mean multiplicities* quoted in Table I which show a small decrease, from a) to d) for low Z, light charged particles (LCP, defined as $Z<3$), products which dominate the total multiplicity. This trend, while the multiplicity of fragments is increasing and corroborates the size decrease of the biggest or residue-like partner, also confirms the presence of quite dissipative events in d). This pleads in favour of a fragmentation of the binary projectile-like target-like subsystem, that is to be related to features mentioned just above for Fig. 3 d_2).

Finally, all above experimental features explain the a priori name attribution of the different cuts a) to d), and particularly the pure single (poly) source one for the a) (d)) sample respectively. Furthermore, similar global features definitely appear to govern and confirm the so-called, on one hand, whole single source bump a) + b), and on the other hand, whole poly source c) + d) bumps. Note that the representativeness of the events selected in the a) or b) regions (respectively c) or d) regions) is not exactly the same as for the selected events in the whole single (poly) source bump. For example, events of the a) region contain more asymmetric partitions than events of the b) region.

The characterization of the evolution of the mechanisms as clearly observed above (from single source fusion-like characteristics to binary-like source scenario), will be studied in more details in the following section.

2. Kinetic and shape variables

The diagrams of Fig. 4 are devoted to the study of shape/kinetic variables gated by the

d_{625} interval	single	single + poly	poly + single	poly
	a	b	c	d
Total Multiplicity	17.5	17.0	16.3	15.1
$Z = 1$ Multiplicity	9.7	8.8	8.3	7.2
$Z = 2$ Multiplicity	5.6	5.5	5.2	4.8
fragment Multiplicity	2.6	3.1	3.3	3.6
$<Z_{tot}>$fragments	28.3	29.2	31.0	32.8
$<Z_{tot}>$	49.5	49.2	49.7	49.6

Table I: Mean (total, LCP's and fragments) multiplicities, mean total charge of the fragments, and mean total charge of the events, according to the four intervals delimited by the d_{625} discriminant variable (see text).

d_{625} cuts as defined in the previous section. They are expressed in the experimental center of mass (c.m.) of the event. Since we only deal with complete events, the measured velocity in the laboratory (in average $V_{c.m.}$=4.02 cm/ns), is always very close to the one calculated from the initial kinematics, i.e. $V_{c.m.}$ =3.93cm/ns. These plots represent (from top to bottom) : coplanarity versus sphericity, charge versus parallel (to the beam axis) velocity, perpendicular (to the beam axis) versus parallel velocity, and mean fragments kinetic energies ($\langle E_{kin} \rangle$) versus their charge (Z).

- The first row displays the *coplanarity (C) versus sphericity (S)* plots. Such global variables are related to the event shape. These plots indicate that the single-source events selected by the d_{625} criterion (Fig.4, a_5)) show spherical shapes ($S \sim 0.7$). This indicates a more isotropic single-source emission than on the opposite in case d_5), where the binary-like selected events appear more concentrated close to the elongated shape corner ($S \sim 0.4$).

- In the second row, the behaviour of the *charge versus parallel velocity V_{par}* reveals from a_6) to d_6) a spectacular change in the mechanism. Indeed in Fig. 4 a_6), the picture exhibits a single-source emission pattern globally centered on the c.m. However, a fraction of the light ($Z \leq 8$) fragments appear a bit more concentrated at the forward of the c.m. while the heavier fragments, with $Z \geq 15$, lie at a velocity slightly negative : this effect is due to detection thresholds. Indeed the plot includes two main components, a high Z one ($15 \leq Z \leq 30$) well defined in both Z and $V_{par} \sim 0$, and a widely spread V_{par} one corresponding to light fragments ($Z \leq 8$) and numerous LCP's. There is a depletion of fragments with $Z \sim 8$ to ~ 15 between these 2 components, as already observed in Fig. 3 a_1). A continuous evolution is visible through the three other plots, up to d_6) reflecting a binary-like distribution.

The two peaks pointing symmetrically from each side of the velocity V~0, at ± 3cm/ns, correspond to the projectile-like and target-like contributions. Both peaks contain charge with Z ranging mainly from ~13 up to $Z \sim 25$.

- The evolution of the processes is also evidenced through the invariant contour plots, V_{per} (velocity perpendicular to the beam) versus V_{par}, (3rd row), undeniably reflecting the gradual transition from a single-source pattern to a better and better separated bisource one related to the binary-like character of the projectile and the target components.

- Finally, the correlation of particular interest, bottom of Fig. 4, between the *mean kinetic energies* and the *charges* of the fragments ($Z \geq 3$), also reveals completely different underlying mechanisms according to these d_{625} intervals. More precisely, the two lines a_8) to d_8), and a_9) to d_9), concern respectively events without and with a cut on events inside a cone with $\cos \theta = \pm 0.5$ (in the measured center of mass). In addition, empty squares and dark triangles symbolize events with and without the heaviest fragment respectively.

As it can be seen in Fig. 4 a_8), for the heaviest fragment (from $Z \sim 14$ to $Z \sim 32$) the mean kinetic energy remains low and is slightly decreasing (from ~30 to ~20 MeV). This behaviour is then assimilated to an evaporation residue pattern, compatible with an incomplete fusion scenario followed by a sequential evaporation process. It is interesting to stress this particular energy slope breakdown (from ~ 70 to ~ 30 MeV) between $Z \sim 10$ and ~14, where the charge yields are the lowest as observed above in Fig.4 a_6) and Fig.3 a_1). This point will be discussed in section V.

The pure poly-source events (in d_8), on the opposite, exhibit a strong increase, from ~40 to ~180 MeV. Increasing kinetic energy with charge can be obviously attributed to a domi-
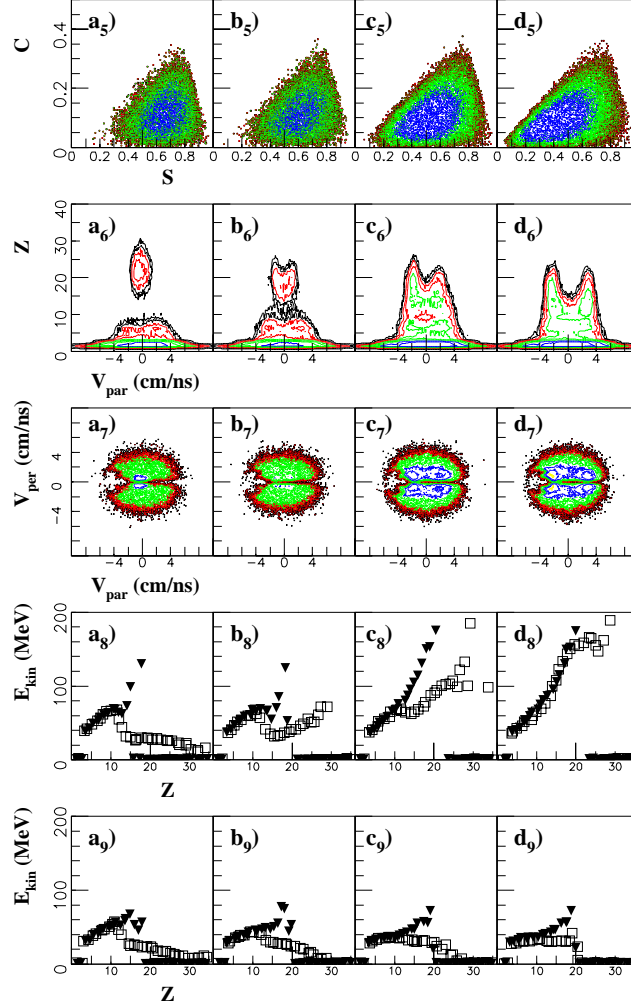
Figure 4: *Kinetic variables* evolution, according to the same d_{625} intervals as in fig.3). Coplanarity versus Sphericity (a_5-d_5), Charge Z versus parallel velocity (a_6-d_6) (for the first three rows, axis z corresponds to a logarithmic scale), V_{per} versus V_{par} (a_7-d_7), mean kinetic energy E_{kin} of each fragment *with* (open squares) and *without* (black triangles) the Z_{max} of the event (a_8-d_8). The last row stands for the same E_{kin} as above but with a cut on forward/backward angular region (see text). Note that the plots are normalized to the number of events (excepted a_3-d_3) independantly for each plot.

nant binary character of the collision, keeping memory of the entrance channel, specially for the heaviest ($Z \geq 16$) products. These fragments are related to the less dissipative component of the binary mechanism.

For comparison, we now consider the same curves (a_8) to d_8)) but with the heaviest fragment of the event removed (dark triangles). These curves clearly enhance the completely different behaviour of the pure single-source events with respect to the others. When the heaviest fragment is removed, no fragment with charge over 14 is observed in the pure single-source events (the apparent rising up

for $Z \sim 15$ to ~ 17 is not significant since it corresponds to very low statistics), whereas fragments with charge up to 22 are still observed in the pure poly-source events. This shows that in pure single-source events a quite heavy residue can be still observed, whereas most pure poly-source events contain two heavy fragments.

Coming back now to these numerous lighter fragments, $Z \sim 3$ to ~ 10 we note that on the opposite, their mean E_{kin} steadily increase from ~ 40 up to ~ 70 MeV. Moreover, this behaviour, which seems to keep the same increase $\langle E_{kin} \rangle$ with the charge whatever the d_{625}

interval, a_8) to d_8), i.e. whatever single(poly)-source involved, hence over a rather large impact parameter range, is worth to underline. This trend was already observed in the heavier Xe+Sn system at 50 MeV/nucleon [19]

As a check on the reliability of the data, the angular cut (as defined above) performed in the pure binary case of Fig 4 d_8) and d_9), exhibits on the opposite a spectacular change. Indeed, the strongly increasing $E_{c.m.}$'s from 40 MeV (Z=3) to 160 MeV ($Z \sim$23) (empty squares and full triangles standing for with and without Z_{max} respectively) is suppressed by the angular cut, as expected from such binary collisions with a strong memory of the entrance channel. Indeed it is replaced (in d_9)), and for both symbols, by a wide plateau extending from Z =3 to $\sim$20 with constant $\langle E_{c.m.}\rangle > \sim$30 MeV. Such a behaviour reflects the presence of some transverse energy contribution due to the most dissipative collisions in d), as previously observed for example in the heavier Xe+Sn system at 50 MeV/nucleon [19].

These features are also confirmed in the data obtained with such angular cut performed on Z_{max} plot, where the very less dissipative binary component (above $Z_{max} \sim$ 17 in Fig. 3, d_2) and d_3)) is found to disappear, thus leading to enhancement of the most dissipative one around Z_{max}=12 (and even, to a lesser extent, around Z_{max}=8.)

The diagrams of Fig. 5 show in more details the single a) and poly-source b) patterns respectively, for Z=1 and 2 particles and for the *charge density* (i.e. velocity diagram weighted by the Z charge of all products). These patterns are confirmed both for Z=1 and 2 particles, while in addition the charge density diagrams emphasize these trends for all fragments and particles. One can remark however that the poly-source pattern exhibits a "mid-rapidity" emission especially for the Z=2 case. It is observed, in Fig 5, that this contribution disappears in the fragment case (i.e. the fragment density at mid-rapidity is lower than 1/30 of its maximum).

To summarize, this overview of experimental observables demonstrates the efficiency of the D.A. method and its related d_{625} variable, to clearly disentangle a major presence of single-source events for the lowest values of this variable, from dominant bi-source ones for its highest values. It might be noted that all this topology was already visible in the raw data of Fig. 2 when comparing the proposed pure single-source and pure poly-source labels.
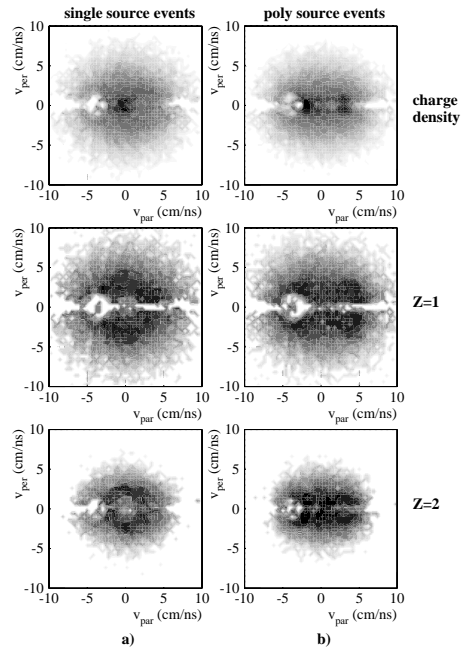

Figure 5: *Velocity diagrams V_{per} versus V_{par} for single-source events (interval a)), first column, and for poly-source events (interval b)), second column, in 3 cases : each fragment weighted by its charge, Z=1, Z=2 (rows 1, 2 and 3 respectively, axis z with a logarithmic scale).*

We have now to further characterize the selected pure single-source events which present strong features of a fusion-like process, suggesting from the above experimental study the formation of a highly excited subsystem. Indeed, quite a large energy dissipation can be observed from these 32 MeV/nucleon Ni+Ni collisions, whatever the involved subsystem, relevant of a single- or poly -source pattern. The hypothesis of a hot compound system will be discussed in the next section where the analysis is focused on the pure subset of single-source events.

IV. SINGLE SOURCE CHARACTERIZATION

We have been able, with the d_{625} description of our data, to sort out pure single source events, giving strong support to a well defined emitter. As mentioned in section III B), the very clean selection favours more

asymmetric partitions in the exit channel. The nature of this source will be determined with more precision, particularly via a study of emission processes leading to the final products.

A. Equilibrium and pre-equilibrium emission

A simple way to look for *thermal equilibrium*, as involved for example in the evaporative process of a hot source as just mentioned above, is the Maxwellian and isotropic behaviour of the particle energy spectra.

We shall examine afterwards more quantitatively the deviations from such a supposed isotropic particle emission, which could be due to pre-equilibrium effects. For that purpose the total experimental angular region has been divided into 8 domains determined as in [3], in the c.m., in order to cover equivalent solid angle sectors.

In a first step, taking into account that the non-equilibrium effects are mostly expected at forward/backward angles (symmetric systems), this anisotropic component will be excluded from the angular distributions, by suppressing particles emitted outside a cone between $\theta_{c.m.}$ = 60° and 120°. Then the related four sectors cover the intermediate angular range, i.e. part "B" (Figs. 6-7), whereas part "A" is concerned with the four extreme backward and forward angular sectors. Energy distribution spectra from part B are displayed in Fig. 6 for the various LCP's and fragments. In these conditions one observes quite similar slopes for protons, deuterons, tritons and alphas (see Table II) as expected from equilibrated emission (note that the slope for Z_{max}'s is close to the one of light particles). This feature is reinforced in Fig. 7 where, in part B, the four sector energy distributions of $Z = 1$ (left column) and $Z = 2$ (right column) particles are put together : they appear quite superimposable, opposite to part A which includes the four extreme backward and forward angular sectors. Indeed, these similar slopes in B reflect (Fig. 6), a same apparent mean "temperature" as quoted in Table II, i.e. around $T \sim 10\text{-}11$ MeV for LCP's (surface or volume emission formulations lead to comparable "temperature" results, though fits are better for the low energies ≤ 20 MeV with a surface emission, while a volume one better accounts for the higher energies). We remark at this stage that these temperature parameters appear relatively high for a pure sequential de-
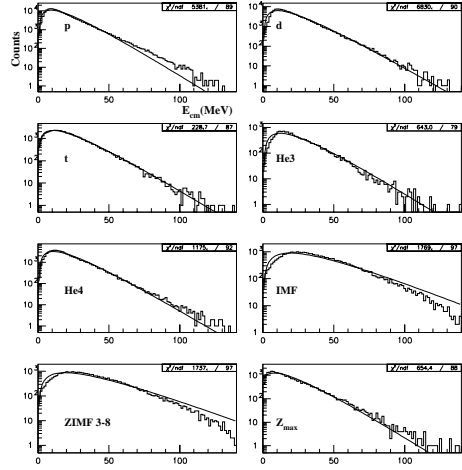

Figure 6: Center-of-mass energy distributions (histograms) for protons, deuterons, tritons, He3, α's, fragments, light fragments (3<Z<8), and Z_{max} for $60^o \leq \theta_{cm} \leq 120^o$ (part B). The continuous lines stand for Maxwellians adjusted distributions (surface emission type).

cay scenario, while the light fragments involve a much higher T_{app} as reported in Table II.

However, the mean kinetic energies of the concerned species reported in Table II are compatible with expected values from a statistical emission calculation as performed by the Simon code used in its standard statistical sequential decay approach. One may notice (Table II) no significant deviation, for the ^{3}He particles mean kinetic energy, from the other experimental light particle values. However, they exhibit a rather different shape at the beginning of their energy spectra where the small energy component is suppressed, compared to the other particle spectra. Such ^{3}He specificity has previously been pointed out in INDRA data, [21], where this effect was found much more pronounced through a study of a heavier and more energetic system, and attributed to an early ^{3}He emission from the hot compressed compound nucleus.

For the slopes of each class of particles, a hierarchy is observed in the emission of the different products. Light fragments appear to be issued from a more excited system than α's and protons, as expected from statistical emission involving sequential decays as well as prompt multifragmentation.

In a second step, in order to better define the emitter, we need to get more quantitative information about the above mentioned *pre-equilibrium* stage of the reaction. For that

particle	p	d	t	^{3}He	α	$3 \leq Z \leq 8$	Z_{max} only	all fragments
$<E_{exp}>$ (MeV)	18	20.5	21	23.5	21	37	19	30
$<E_{simon}>$ (MeV)	19	23	22.5	25	24	—	—	—
T_{exp}^{app}(MeV) Surf.(Vol.)	9(11)	10(11)	10.5(12)	11.5(12)	10(12)	18.5(18)	11(12.6)	19(18)

Table II: Equilibrated emission (part B) : Particle mean kinetic energies compared to the expected values from a classical statistical emission and "apparent" temperatures from Maxwellian fits ("Surf." for surface, "Vol." for volume).
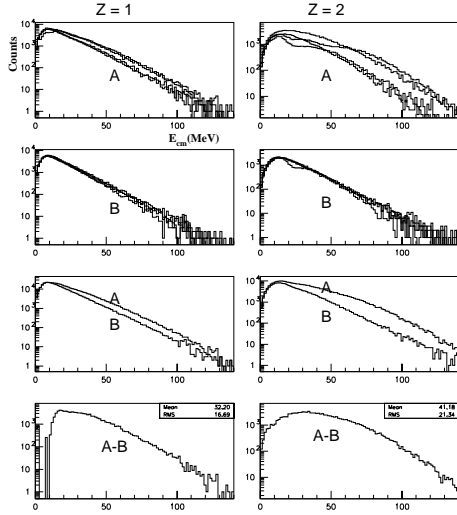

Figure 7: Center-of-mass Z=1 (left column) and Z=2 (right column) energy spectra for various angular domains (see text) :
-Part A) extreme angular sectors ($\langle 29^o \rangle$, $\langle 50^o \rangle$, and $\langle 129^o \rangle$, $\langle 151^o \rangle$).
-Part B) intermediate angular sector ($\langle 68^o \rangle$, $\langle 83^o \rangle$, $\langle 97^o \rangle$, $\langle 112^o \rangle$).
(note that the irregularity induced by the detector, observed for Z=2 at backward angles does not affect the difference (A-B) in the last row).
-Third row : A and B summed angular sectors.
-Last row : center-of-mass subtracted energy spectra for emitted pre-equilibrium.

purpose we consider in Fig. 7 the energy spectra of Z= 1, 2 products emitted in parts A and B described above. The particle emission in sector A, which involves the four most backward/forward regions, appears clearly to deviate, mainly at extreme forward/backward angles, from isotropy. Obviously part A appears to include a pre-equilibrium contribution. Therefore, subtracting the thermal component observed in part B from part A, leads to a reasonable good estimate of the pre-equilibrium energy spectra. The Z=1 pre-equilibrium energy spectrum reveals (Fig. 7, bottom) a dissymetric component of energetic particles pointing around $E_{c.m.}\sim$18 MeV but with a mean value at $<E_{c.m.}>\sim$32 MeV. Among these Z=1, the proton emission, which

is dominant,($\sim$55%), would then correspond to a mean velocity of $\sim$7.5 cm/ns, i.e. $\sim 2.V_{c.m.}$ (3.93 cm/ns). We have observed that the total $E_{c.m.}$ mean values for deuterons and tritons are roughly the same as for protons, i.e.. around 30 MeV. The same procedure applied to the Z=2 pre-equilibrium emission particles leads to a broader and more symmetrical distribution, centered around $<E_{cm}>\sim$40 MeV, corresponding to $\sim$ 4.3 cm/ns for dominant α's particles, i.e. $\sim 1.1 V_{c.m.}$.

These differences between pre-equilibrium protons and alphas imply that their emission dynamics are not the same. We may suggest, as shown in [22], that such energetic protons extending up to $\sim$110 MeV, (the kinematical limit being $\sim$80 MeV) are mostly emitted through N-N collisions in the first stage of the reaction [23]. Similar interpretation of the α emission is not so obvious and could be related to this peculiar process previously observed in central collisions i.e. the so-called "spray" effect [5, 7], responsible of α and light fragment forward emission in a fusion-like process. Indeed, it has been shown for the ^{40}Ar+Cu, Ag, Au for 17-115 MeV/nucleon incident energy, that the initial composite system mass decreases with energy also, but by a relatively small amount. These central collisions can be said to change gradually from incomplete fusion with capture of most of the projectile to "splintering" central collisions with capture of only a small fraction of the projectile nucleons. The early reaction dynamics generate a multibody spray of nucleons and fragments ejected in the forward direction (i.e., that of the Ar projectile). In the present work, some light fragments (from Z=3 to $\sim$8) are also observed, at $<E_{cm}>\sim$59 MeV, but with a so low statistics that this last emission is neglected in the following. Hence, if it exists, such a spray effect will not be taken into account in this Ni+Ni medium size system at 32 MeV/nucleon incident energy.

As we need to obtain an event by event estimate of a global charged pre-equilibrium emission, we have attempted different procedures to deduce these experimental quantities. First we have considered the subtraction A-B

for each species (see Fig. 7) relatively to its total yield A+B (i.e. $\leq 20\%$ for $Z=1$ and $\sim 30\%$ for $Z=2$). Another method lies on the integrated Maxwellian fitted curves. A third one is based on the shape of the angular distributions. Lastly, we have followed the prescription of [24]. Hence, it is important and comforting to stress that whatever the method, all the deduced estimations for charged pre-equilibrium components converge towards similar values such as :

$Z_{pre-eq} \sim 7$ charges, with a charge multiplicity dispatched as : $M_{Z=1} = 3$ and $M_{Z=2} = 2$

These values are corrected from the detector bias.
Finally this estimation will help to determine the size and excitation energy of the source, as presented in the next paragraph.

B. Size and excitation energy of the single-source

We have now to add the neutron contribution to the experimentally deduced total Z_{pre-eq} emitted *charge*, in order to extract the total amount of non-equilibrated emitted matter, and then to evaluate the *size* of the source.
The number of pre-equilibrium neutrons can be evaluated using two different prescriptions. On one hand it is reasonable to suppose that the isospin equilibration is realized at the first instant of the reaction by ejecting the four exceeding neutrons. On the other hand, the N/Z ratio can be considered as remaining the same in the preequilibrium component as in the entrance channel. Both assumptions lead to compatible values which can be estimated at about 9 ± 2 neutrons. The minimum amount of pre-equilibrium emitted *mass* is then deduced as :

$A_{pre-eq} \sim 16$ mass units, thus leading to a size of the source :

$A_{source} \sim 100$, (since $A_{tot}=116$ and $Z_{tot}=56$) with $Z_{source} \sim 49$

Table III displays the results of this estimate, together with the estimates for protons and neutrons given by various predictions : Simon, Blann's [25] and BNV [26] models. We remind that in such models, the pre-equilibrium calculation is performed only for nucleons. There-

	$Z = 1$	neutrons
Simon code	6 ± 1	6 ± 1
Blann code	6 ± 1	10 ± 2
BNV code	4 ± 2	4 ± 2
experiment	7 ± 1	9 ± 2

Table III: Pre-equilibrium emission (part A): mean numbers of total emitted *charges* and *neutrons*. Predictions and experiment.

fore, the comparison makes sense only for the total emitted charge. Both the Simon and the Blann's codes provide a quite quantitative agreement with the data .

The *excitation energy* stored by the single-source has been evaluated by a calorimetric method [27], after subtraction of the pre-equilibrium component estimated just above. This method takes into account the Q-value of the reaction, the kinetic energies of detected products, an estimated energy for the neutrons and a residual excitation energy of the hot nucleus. As a result, a mean value of $<E^*> \sim 500$ MeV, or still $<E^*> \sim 5$ (± 0.8) MeV/nucleon for a total mass number of the emitter $A_{source} \sim 100$ is obtained .
Since the total available energy in the Ni+Ni system at 32 MeV/nucleon amounts to 835 MeV in the c.m., i.e. ~ 7.2 MeV/nucleon, this leaves $E_{pre-eq} \sim 335$ MeV for the energy carried out by the pre-equilibrium emission.
According to our deduced pre-equilibrium yields and related mean kinetic energies (Fig.7), we then obtain values compatible with the one deduced just above.
This measured excitation energy per nucleon of the fusion-like nucleus is relatively high and moreover, close to the multifragmentation threshold defined as the passage from dominant two-body to multi-body splitting of hot heavy nuclei [8]. We underline that our data could then extend such a description to medium size symmetric systems.

In summary, it comes out that most of the incident mass (~ 86 %) and only about half of the initially available energy($\sim 55\%$) of the system is devoted to the formation of a relatively hot and equilibrated subsystem. Hence, it is the early emission of prompt light particles which permits to form the excited composite nucleus. We now examine its decay modes.

V. CHARACTERISTICS OF THE DECAY CHANNELS

A fundamental question raised in the phenomenology of multiple fragment production lies in its evaporation-sequential or multifragmentation-simultaneous character. The latter sets a link with the equation of state whereas the sequential case refers to an extension of the standard and dominant evaporative decay mode, as observed for a long time at lower incident energies (≤ 20 MeV/nucleon, where a heavy residue is accompanied by LCP's). An interesting process could be a phase coexistence reflected by a bimodality of the event distribution.

A. Sequential decay

A strong indication of such fusion-like/sequential evaporation process can be seen in Fig. 8 which displays the two-dimensional plots of the charge Z of each fragment as function of its velocity expressed in the c.m. frame. The left plot a), shows the same correlation as in Fig. 4 a_6), but including only fragments, while the right plot b) illustrates the case where the heaviest fragment Z_{max} of each event has been excluded : we clearly observe only remaining low charge fragments ($Z \leq 12$) with velocities spread between $\sim \pm 4$cm/ns (i.e. $\pm V_{proj}$). Moreover, the study of these selected events shows that they all include systematically one relatively heavy fragment around the c.m. velocity. The mean charge of the heavy fragment stands around $\langle Z_{max} \rangle$ = 22 ranging from ~ 12 to ~ 35 (Fig. 3 a_2). Moreover, in this high $\langle Z_{max} \rangle$ value region, the mean kinetic energy ($\langle E_{c.m.} \rangle$) of the fragments (see Fig. 4 a_8) is low and slowly decreasing with $\langle Z_{max} \rangle$ increasing. Thus this feature a priori would support a standard evaporation type of scenario, leaving a relatively heavy residue, with numerous LCP's and also some IMF's (Intermediate Mass Fragments are defined as fragments excluding the heaviest product). However, we may remark that this $\langle Z_{max} \rangle$ mean value would correspond to a rather low size residue-like value as compared to $Z_{source} \sim 50$ and to a total fragment emitted charge $\langle Z_{tot} \rangle \sim 28$. This is all the more true for the events in which the heaviest fragment has a charge as light as 15.

We now turn back to the charge asymmetry, $Asym_{123}$, distributions of Fig. 9. The slight peaking at the highest values i.e. ~ 0.8 was
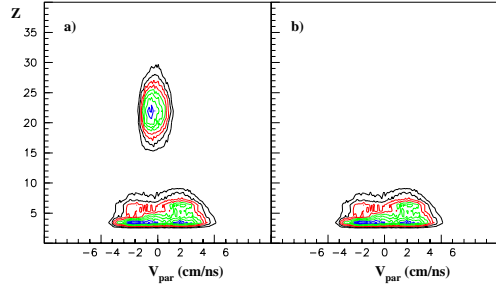
Figure 8: Charge velocity diagram $with$(a)) and $without$(b)) the heaviest fragment (for the two plots, axis z corresponds to a logarithmic scale).

already pointed out as characterizing a pure sequential decay component. Indeed this relatively weak structure corresponds to the highest values of Z_{max} accompanied by the very lowest Z_{max-1} values ($Z \leq 3$), corresponding to the lowest islet in Fig. 3 a_3). However, it constitutes only a small part of the whole $Asym_{123}$ distribution, the remaining dominant part being spread around 0.6 and related to the events which include a relatively light Z_{max} accompanied by fragments (mostly with $Z \sim 4$ to ~ 8) and LCP's. Nothing being left at $Asym_{123} \leq 0.3$, we do not observe nearly equal size events as we might have expected in the framework of a spinodal process [28].

Finally we have shown that the decaying process, for the Ni+Ni system at 32 MeV/nucleon presents, at least for a significant part of the sample, some typical characteristics of an evaporative scheme. This is clearly evidenced in Fig. 8 and for the events belonging to the relatively small and narrow peak at the largest asymmetry ($Asym_{123} \sim 0.8$) values (Fig. 9). This structure corresponds to events involving mostly a residue of size $20 < Z < 35$ and LCP's and represents about 10% of the single-source events. They indeed may be considered as pure sequential evaporative decays.

The Gemini [29] code - which describes the single-source emission within the framework of sequential decay - has been used with input parameters equal to the values deduced above for the single-source size ($Z = 50$, $A = 100$) and excitation energy ($E^* = 5$
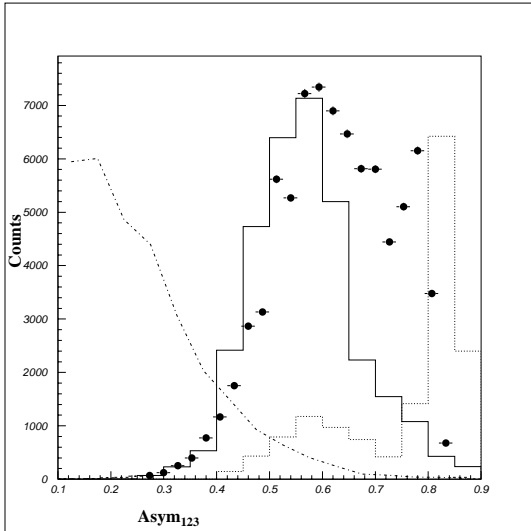
Figure 9: Charge Asymmetry ($Asym_{123}$) : black dots stand for the data. The model distributions SMM (full line histogram), GEMINI (dotted line histogram) and random mass partitions (dashed-dotted line) (see text).

MeV/nucleon). It indeed reproduces, as shown in Fig. 9, large asymmetries (dotted line) with a strong dominating peak at $Asym_{123}\sim0.8$, but fails to describe the major part of the experimental distribution centered around $Asym_{123}\sim0.6$. The confrontation of Gemini with experimental data has shown that, at high excitation energy, this model overestimates the production of light particles. This explains the small shift between our experimental peak and the Gemini peak. Hence we confirm the evaporation-sequential character of a part of the single-source decays with charge partition $Asym_{123}$ lying around 0.8 .

Furthermore, to check these data against a possible trivial peaking, the so-called Dynamic Minimum Hypothesis, DMH, (Monte-Carlo calculations) has been developed [30]. The input parameters of this toy model are the total charge and the excitation energy (here Z_{tot} = 50 and $E^* = 5$ MeV/nucleon). The charge partitions are generated through the hypothesis that all possible partitions from Z_{tot}, compatible with the available energy, have the same probability (minimum information model). Energy and momentum are conserved event by event.

These DMH events are filtered in order to account for the detector biases. We observe that the experimental splittings depart clearly from this minimum biased simulation (dashed-dotted histogram Fig. 9). This confrontation

shows that the structure at $Asym_{123}\sim0.6$ cannot be accounted for by some fortuitous filtering or combinatory effects in the mass partitions .

Therefore, an alternative process, departing from the classical evaporation sequential picture, has to be invoked in order, for example, to satisfactorily reproduce the observed overall asymmetry distribution. The correlative question is to identify the multiple fragment de-excitation mechanism corresponding to this dominant remaining part of the data sample.

B. Multifragmentation from phase coexistence ?

To hunt for this de-excitation mechanism the experimental sample is confronted with a Statistical Multifragmentation Model (SMM) [31]. SMM has been used with the same input parameters as Gemini and the same criteria as for the experimental data have been applied. The results for the $Asym_{123}$ distribution is shown in Fig. 9 (full line). The dominant stucture at $Asym_{123}\sim0.6$ can be rather well reproduced, whereas the narrower structure at $Asym_{123}\sim0.8$ is not accounted for. This latter structure being reproduced by the Gemini distribution but with a rate much greater than in the experimental distribution, we try, as in [2], to mix the two processes. A proportion of 90% of SMM events and 10% of Gemini events is found to satifactorily reproduce the data.

This duality in the data between evaporative and simultaneous multifragment emission agrees with previous analyses [1, 8] which locate the onset of simultaneous multifragmentation around 30 MeV/nucleon incident energy. Moreover, a significant amount of collective motion has been shown to appear [1] beyond a beam energy of about 30 MeV/nucleon, for heavier central symmetric collisions, at excitation energies greater than about 5 MeV/nucleon. This is to be related with the suggestion [8] that the transition from sequential to simultaneous fragmentation, i.e. from decay at normal density to disassembly at a lower density, is expected to be coupled with the onset of matter expansion. At this stage we stress that the analysis of mean kinetic energies constitutes an experimental signature for radial auto-similar collective motion. We observe in Fig. 4 a_8) that the light fragment energy increases with the charge. This effect, difficult to explain in an evaporative scenario (see above), clearly recalls the behaviour
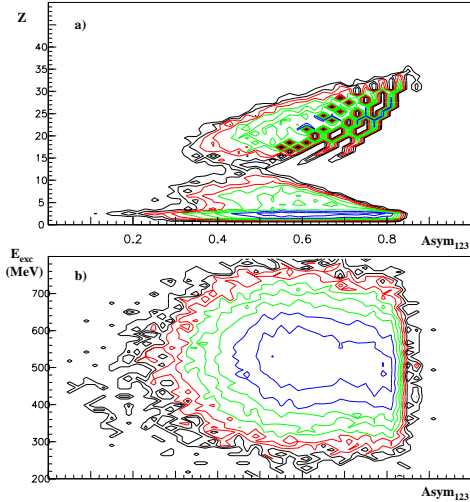
Figure 10: Asymmetry versus : a) Charges Z of the fragments/particules of each event, or so-called "butterfly plot", and b) measured available excitation energy E_{exc} of the composite subsystem (for the two plots, axis z corresponds to a logarithmic scale).

of the lighter fragments in symmetric heavier systems such as Xe + Sn [3, 19, 32] and Gd + U [9] around 32 and 50 MeV/nucleon incident energy. In these latter systems it was shown that a small radial expansion energy was required, from 0.5 to around 1 MeV/nucleon at ~30 MeV/nucleon incident energy, to around 2 MeV/nucleon at 50 MeV/nucleon incident energy. In our case, the result obtained with the SMM model is compatible with no radial expansion energy to explain the distibution in Fig. 4 a_8). However, a small expansion component is hardly measurable, as discussed in the case of heavier systems [9, 32].

Therefore, that interesting double aspect (sequential decay and thermal prompt multifragmentation) is presently clearly evidenced for the first time for such medium size symmetric system as Ni+Ni at 32 MeV/nucleon incident energy; it has also been shown recently for a heavier system, Ni+Au at 32 MeV/nucleon [33]. This duality is also represented Fig 10 a). In this "butterfly" shape, each charge is correlated to its $Asym_{123}$ value. The highest $Asym_{123}$ values essentially correspond, in a narrow domain, to the largest residue-like size, accompanied by LCP's. On the opposite, the dominant remaining part is widely spread, progressively extending with decreasing $Asym_{123}$, towards more fragments but with a depletion (already mentioned above) around $Z=10$ which progressively fills in.

This duality could hold in the framework of a threshold effect : the onset of a new mechanism (instantaneous multifragment emission) in place of the vanishing evaporative one. However, in this scenario, one might expect a dependence upon the convertible energy : an instantaneous multifragment process should correspond to higher excitation energies than a sequential process. This difference should be visible in the data. To check this effect, we have plotted (Fig. 10 b)) the measured available excitation energy in the composite system versus the $Asym_{123}$. The plot presents a very interesting feature : the two regions of events corresponding to the two different asymmetry domains discussed above appear at almost the same excitation energy (~500 MeV). The fact that we do not see any pronounced correlation between the charge asymmetry pattern and the excitation energy, implies that, for the selected sample, the charge partition is not governed by this amount of available excitation energy. Indeed, such a two component decay process cannot be so simply related to the fluctuations of the amount of energy relaxed by pre-equilibrium emission. We emphasize that for such a hot subsystem various channels are open. Then a high excitation energy might not necessarily be the signature of a prompt multifragmentation alone, but could be compatible with the co-existence of both decay processes driven by *thermal* fluctuations.

Then, the remaining question is to know if the duality in the experimental results is related to a phase transition signal. As explained in [34, 35], an extended definition of first order phase transitions in finite systems generalizes definitions based on curvature anomalies of any thermodynamical potential as a function of an observable which can then be seen as an order parameter. It gives an understanding of coexistence as a bimodality of the event distribution, each component being a phase. It provides a definition of the order parameter as being the best variable to separate the two maxima of the distribution. In this framework, when a nuclear system is in the coexistence region, the probability distribution of an order parameter is bimodal and large fluctuations in the partitions of the system can be observed [34–36]. Experimentally the width of the $Asym_{123}$ fluctuations, seen in Fig. 10 b), represents about the 2/3 of the whole asymmetry distribution. Moreover, the bimodality of the event distribution can be seen in Fig. 9, between the events well reproduced by the SMM model and those well reproduced

by the Gemini model. Hence, the Asym_{123} variable can be seen as an order parameter since it shows a two bump distribution which separates two decay processes. Nevertheless, it is likely that other variables could be defined in order to obtain a better separation. Such complementary analyses are required.

VI. SUMMARY - CONCLUSIONS

In this paper, we have focused on the characterization of single source sample from $^{58}\text{Ni}+^{58}\text{Ni}$ collisions at 32 MeV/nucleon, using a set of complete events recorded by the multidetector INDRA. The high performances of this 4π device combined to a quality method of event selection, have lead to a large set of well characterized data. Indeed, the original Discriminant Analysis procedure, involving multivariate moments, was definitely proved as an efficient tool to clearly disentangle a single-source contribution from much dominant binary-like dissipative collisions. The investigated four selected cuts (from pure single-source events to pure poly-source events) reveal in each case a relatively high energy dissipation. Moreover, a continuity is observed as a function of the appropriate d_{625} discriminant variable between the former and the latter, for static and kinematic variables.

The fusion-like subsystem endeavours a statistical multiple-fragment decay after thermal equilibrium has been reached. The role of the pre-equilibrium emission has been investigated. On one hand, about 16 mass units are ejected, i.e. about 14% of the total incident mass. Then, a large part of the initial mass is stored in the subsystem with a mean charge lying around $Z_{tot} \sim 49$ charge units. On the other hand, the pre-equilibrium emission leaves nearly the half of the convertible energy stored in the subsystem. Nevertheless, its excitation energy corresponds to about 5 ± 0.8 MeV/nucleon which involves a hot subsystem close to the prompt multifragmentation onset.
Surprisingly, events with $\langle Z_{max} \rangle \sim 22$ plus light particles and/or few light IMF's still exist and are well reproduced by a statistical sequential decay model (Gemini). It represents about 10% of the single source events. The dominant remaining class of events ($\langle Z_{max} \rangle \sim 12$ plus light particles and IMF's) is well reproduced by a statistical simultaneous multifragmentation model (SMM). This coexistence characterizes the transition region from the standard fusion-evaporation process which is supposed to leave a final heavy cold residue plus light fragments and/or particles, towards a thermal prompt multifragmentation scenario producing fragments of more similar sizes.
Moreover, this duality between a pure evaporative component and a thermal prompt multifragmentation scheme is clearly evidenced for the first time in a medium size system. For the clean single source selection obtained, which favours the more asymmetric partitions, no radial expansion energy is needed to reproduce accurately the data, and quite the same excitation energy is stored by both class events. Hence this duality can be explained as a bimodality of the event distribution, each component being a phase. In this scheme, the Asym_{123} variable can be seen as an order parameter. Moreover, the large Asym_{123} fluctuations, observed in the partition of the system, also support the hypothesis of an order parameter.
To improve our knowledge on how this steady competition evolves between these two decay mechanisms, complementary studies at incident energies around 30 MeV/nucleon are required. Of special interest is the analysis of the 40 MeV/nucleon $^{58}\text{Ni}+^{58}\text{Ni}$ INDRA data, and even of the higher energy data, presently in progress. These studies should reveal the robustness of the order parameter to sign, in a symmetric medium size system, a first order phase transition.

[1] D. Durand, E. Suraud, and B. Tamain, "Nuclear Dynamics in the Nucleonic Regime", series IOP (2001), and references therein.

[2] A. M. Maskay, PhD thesis, Université de Lyon, France (1999).

[3] N. Marie and INDRA Coll., Phys. Lett. **B391** (1997)15.

[4] M. T. Magda et al., Phys. Rev. **C53** (1996) 1473.

[5] E. Colin et al., Phys. Rev. **C61** (2000) 067602, Rulin Sun et al., Phys. Rev. **C61** (2000) 061601 and Phys. Rev. Lett. **83** (2000) 43.

[6] B. Borderie and INDRA Coll. , Int. Symp. on Advances in Nucl. Phys., Bucharest, Romania(1999),
A. Fhali et al., Phys. Rev.**C34**(1986)161, P. F. Box et al., Phys. Rev.**C50**(1994)934.

[7] E. Colin et al., Phys. Rev. **C57** (1998)1032 .

[8] D. Durand, Nucl. Phys. **A630** (1998)52c and references therein.

[9] J. D. Frankland , PhD thesis, Université de Paris XI Orsay, France (1998) and Nucl. Phys. **A689** (2001)905 and 940.

[10] M. D'Agostino et al., Nucl. Phys. **A650** (1999)329 and references therein.

[11] M. F. Rivet and INDRA Coll, Phys. Lett. **B430** (1998)217.

[12] P. Eudes et al., Phys. Rev. **C56** (1997)2003.

[13] M. Germain and INDRA Coll., Phys. Lett. **B488** (2000)211 and PhD thesis, Université de Nantes, France, (1997).

[14] G. Rudolf et al., Phys. Lett. **B307** (1993)287.

[15] P. Désesquelles et al., and INDRA coll., Phys. Rev. **C62**(2000)024614.

[16] J. Pouthas and INDRA Coll., Nucl. Instr. and Meth. **A357** (1995)418.

[17] P. Désesquelles, Ann. Phys. (Paris), **20**, 1(1995).

[18] D. Durand, Nucl. Phys. **A541** (1992)266.

[19] A. D. Nguyen PhD thesis, Université de Caen, France (1998).

[20] A. Schüttauf and ALADIN Coll., Nucl. Phys. **A607** (1996)457.

[21] R. Bougault et al., in *Proceedings of the XXVII International Workshop on Gross Properties of Nuclei and Nuclear Excitations, Hirschegg, 1999* edited by H. Feldmeier (GSI Darmstadt, 1999)p.24, and W. Neubert and A. S. Botvina, Eur. Phys. J. **A7** (2000)101.

[22] P. Sapienza et al., Phys. Rev. Lett. **87** (2001)072701.

[23] D. Doré et al., Phys. Rev. C 63034612(2001)

[24] P. Désesquelles et al., Multics/Miniball Coll., Nucl. Phys. **A633** (1998)547. and J. C. Steckmeyer and INDRA Coll., Nucl. Phys. **A686** (2001)537.

[25] M. Blann, Phys. Rev. **C31** (1985)1245.

[26] A. Bonasera et al., Phys. Rep. **243** (1994)1.

[27] D. Cussol et al., Nucl. Phys. **A561** (1993)198.

[28] M. Colonna, Ph. Chomaz, and A Guarnera, Nucl. Phys. **A613** (1997)165.

[29] R. J. Charity et al., Nucl. Phys. **A483** (1988)371.

[30] B. Guiot, PhD thesis, Université de Caen, France (2002).

[31] J. P. Bondorf et al., Phys. Rep. **257** (1995)133.

[32] S. Salou, PhD thesis, Université de Caen, France, (1997).

[33] N. Bellaize et al., Nucl. Phys. A 709(2002)367-391

[34] P. Chomaz, F. Gulminelli, and V. Duflot (2001) Phys. Rev. **E64** 046114.

[35] B. Borderie, J. Phys. G : Nucl. Part. Phys.**28**(2002)R217-R247.

[36] R. Botet et al., Phys. Rev. Lett. **86**(2001)3514.